OPEN ACCESS
Journal of Innovative Optical Health Sciences
Vol. 14, No. 2 (2021) 2050026 (9 pages)

DOI: 10.1142/S1793545820500261

World Scientific
www.worldscientific.com

A miniaturized fluorescence imaging device for rapid early skin cancer detection

Jingyue Pan*, Qingquan Liu[†,‡,§], Hao Sun*, Weibo Zheng*, Peiru Wang[¶], Long Wen[¶], Junli Duan[‖], Zhiyi Xuan[†,‡,§], Xiang Yu*, Shaowei Wang[†,§,**,‡‡], Xiuli Wang[¶,††,‡‡], Tao Zhang* and Wei Lu[†,‡,§]

*Shanghai Institute of Technical Physics
Chinese Academy of Sciences
Shanghai 200083, P. R. China

[†]State Key Laboratory of Infrared Physics
Shanghai Institute of Technical Physics
Chinese Academy of Sciences
Shanghai 200083, P. R. China

[‡]School of Physical Science and Technology
ShanghaiTech University
Shanghai 201210, P. R. China

[§]Shanghai Engineering Research Center of Energy-Saving Coatings
Shanghai 200083, P. R. China

[¶]Institute of Photomedicine, Shanghai Skin Disease Hospital
Tongji University School of Medicine
Shanghai 200071, P. R. China

[‖]Department of Gerontology, Xinhua Hospital
Shanghai Jiaotong University
Shanghai 200092, P. R. China
**wangshw@mail.sitp.ac.cn
††wangxiuli_1400023@tongji.edu.cn

Received 29 April 2020
Accepted 9 August 2020
Published 16 September 2020

Fluorescence imaging is very useful for skin cancer lesions detection because of its properties of noninvasion and fast imaging. However, conventional fluorescence imaging devices' excitation light source and camera are usually separated, which will cause problems such as complicated structure, large volume, and poor illumination homogeneity. In this paper, we introduce a miniature portable fluorescence imaging device to diagnose skin cancer. A coaxial design has been

‡‡Corresponding authors.

introduced to combine the exciting light source and fluorescence receiver as an integral part, which significantly reduces the size of the device and ensures illumination homogeneity. The volume of the device is less than $3.5 \times 3.5 \times 9.5\,cm^3$ with weight of 150 g, and the total power (including the excitation lamp) is only 1.5 W. It is used to detect the squamous cell carcinoma mice for demonstration. The results show that the location of the cancer lesions can be easily distinguished from the images captured by the device. It can be efficiently used to detect early skin tumors with noninvasion. It also has prospects to be integrated with other diagnostic methods such as ultrasound probe, for multiple diagnose of skin tumors thanks to its miniature size.

Keywords: Protoporphyrin IX; coaxial design; skin cancer.

1. Introduction

Melanoma and nonmelanoma skin cancer (NMSC) are now the most common types of cancer, especially in the white population, and unfortunately, the incidence of cancer is still rising.[1–5] The public reports estimated an increase from 3.1 to 4.3 million US adults in the treated for NMSC annually from 2002 to 2011,[3] and the incident rates reached to nearly 400 cases per 100,000 people from the Massachusetts All Payer Claims Database in 2015.[5]

In the treatment of all the skin cancers, early diagnosis plays a particularly important role, because skin cancer could turn into invasive growth rapidly and cause high mortality rate if it is not treated in time. Moreover, the early diagnosis can not only improve patient prognosis, but also reduce patient morbidity, as well as treatment complexity and costs.[6,7]

Diagnosis of skin cancer includes histopathological biopsy and various skin imaging methods.[8–11] The histopathological biopsy is the "gold standard" for tissue diagnosis, but it is not suitable for early skin cancer because the characteristics of early skin tumor lesions are not obvious and it is difficult to accurately determine the location and boundaries of the tumor. In terms of skin imaging methods, dermoscopy can magnify the appearance of the tumor and help people to recognize the texture features of pathologic skin based on visual appearance. The reflectance confocal microscopy can highlight the scale characteristics of the skin tumor cells, and the high-frequency ultrasound probe can highlight the depth information of the tumor on the skin surface.[12–14] However, the characteristics of early skin tumors are not obvious, which leads to the inability of ordinary dermoscopy examination to accurately distinguish early skin tumors from normal skin. Moreover, the reflectance confocal microscope and high-frequency ultrasound probe have a very limited view field, and cannot image all suspected tumor sites on a large scale rapidly.

Photosensitizer-mediated fluorescence detection is also known as Photodynamic Diagnosis (PDD).[15–17] It is an effective method for detecting fluorescence using a specific photosensitizer. Protoporphyrin IX (PpIX) is often used in the PDD of nonmelanoma lesions. It is a precursor of heme in its biosynthetic pathway and can emit red fluorescence when excited by the light at about 400 nm. Under normal conditions, heme is regulated and there is no accumulation of PpIX. However, when the precursor of PpIX, such as 5-aminolevulinic acid (ALA) or methyl aminolevulinate (MAL), is applied to the surface of lesion skin, a negative feedback control within mitochondria will change and PpIX will accumulate. Normal tissues can usually eliminate the excessive PpIX very fast, while abnormal tissues have a different form of accumulation and need longer elimination time.[18] Therefore, the lesion can be located by the fluorescence of PpIX.

In recent years, the use of fluorescence-based methods either to detect or to delimitate the invasive extent of several malignant tumors has been widely investigated and enhanced.[19–21]

For example, in 2015, Olena *et al.* reported a study of PpIX metabolism with a handheld fluorescence imaging device that can be easily used in a clinical setting. A corresponding disposable flexible reference frame was fixed to the skin of a patient with tape when analyzing the skin lesion, which allowed imaging the same area through a time-course study.[22] However, they adopted a ring of 16 LEDs powered by a 9 V battery as the source light around the camera, which significantly increased the volume of the device and have high energy

consumption. Moreover, it also needs to install and unload the filter repeatedly to obtain the PpIX emission image and normal image of the skin. Also in 2015, Clovis *et al.* reported a device consisting of two probes — one emitting 630 nm light was used to do the photodynamic therapy (PDT) treatment and the other emitting 450 nm light was used to excite the fluorescence of PpIX. A handheld filter was used to help doctors observe the skin lesions illuminated by the 450 nm light.[23] It can be used for both treatment monitoring and PDT treatment, but it requires the user to observe with the naked eyes, which makes the observation method inconvenient and might damage the user's eyes because of the blue light emission.[24]

Those reported results show that fluorescence imaging has the advantages of fast and real-time imaging. However, their light source is separated from the fluorescence imaging camera, which results in an illumination homogeneity problem, large volume and high energy consumption. Moreover, every technology has its limitations, such as low penetrating for fluorescence imaging and low resolution for ultrasound imaging. The combination of skin imaging technologies has become a promising direction to overcome their shortages. When combining the fluorescence imaging and ultrasound imaging techniques, they can locate the lesion and acquire depth information and even provide three-dimensional information of the tumor. They can get more information from the lesions and help clinicians diagnose more accurately.[25,26] The combination of skin imaging technology with others also requires the miniaturization of the device. Therefore, we report a miniature portable fluorescence imaging device with a coaxial path for illumination and fluorescence to reduce the size, lower the power and solve the illumination homogeneity problem. As a demonstration, the device is used to distinguish the early skin cancer tumors of mice successfully.

2. Fluorescence Imaging System

The separation of light source and acquiring system in most fluorescence image acquisition devices is the main obstacle for their applications as mentioned above. In our device, we propose a coaxial optical path for illumination and fluorescence to integrate the light source with camera tightly, as shown in the principle diagram of Fig. 1(a). The fluorescence imaging device consists of three parts: A LED light source, a fluorescence acquisition part, and a coaxial light path. They will be introduced in detail as follows.

The fluorescence acquisition part mainly includes a CMOS image sensor, a field programmable gate array (FPGA) chip, a static random-access memory (SRAM) chip, a data transmission interface and a power supply circuit. These components are integrated on a Printed Circuit Board (PCB) and are

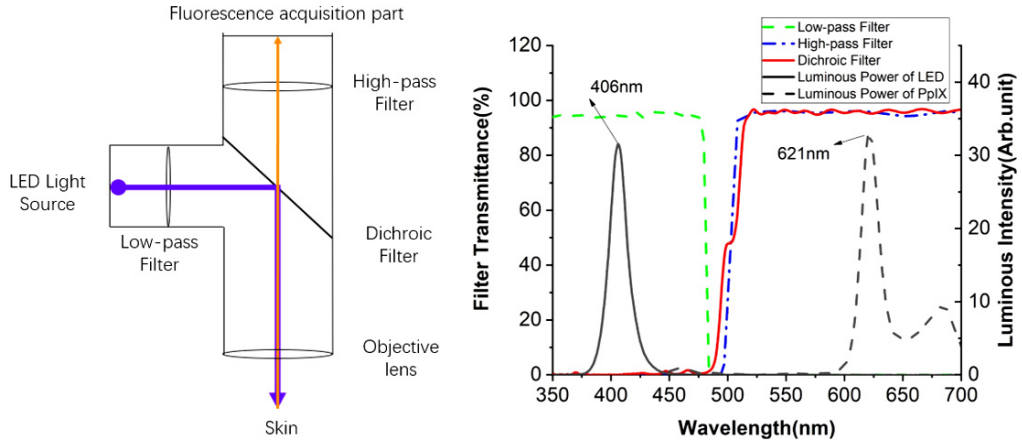

(a) (b)

Fig. 1. (a) The principle diagram of the miniaturized fluorescence imaging device we proposed. The wide blue line is the excitation light, and the narrow orange line represents the fluorescence light. (b) The transmittance of the filters, and the luminous intensity of the LED and PpIX fluorescence. The green dash line is the transmittance of the low-pass filter; the blue dash-dot line is the transmittance of the high-pass filter; the solid red line is the transmittance of dichroic filter; the solid black line is the luminous intensity of LED, its peak is at 406 nm; the black dash line is luminous intensity of PpIX fluorescence, its peak is at 621 nm.

responsible for the acquisition and transmission of image data. The light source is a LED with a wavelength shorter than the fluorescence of PpIX. We choose a blue LED with a peak wavelength of 406 nm in this case and it is perpendicular to the CMOS sensor in the light path. The illuminous intensity of LED is shown in Fig. 1(b) with black solid line. The coaxial light path composed of three filters: A low-pass filter, a high-pass filter and a 45° dichroic filter. The low-pass filter is used to filter out the long-wavelength light from the source and environment. The high-pass filter is used to filter out the source light which is reflected from the skin to emphasize the fluorescence signal of the object. Dichroic filter is an important component to combine the illumination and fluorescence paths, which can reflect the short-wavelength light and transmit the long-wavelength light simultaneously. Therefore, the source light will be reflected to the skin to excite the fluorescence. The excited fluorescence signal from the skin will transmit through it and reaches the image sensor. The coordination of these filters ensures the integration of two optical paths, resulting in the simplified structure and reducing volume remarkably. It also prevents the interference of illumination and ambient light to ensure the acquisition of pure fluorescence information from the object. The transmission spectra of the filters and the luminous power of PpIX fluorescence are shown in Fig. 1(b). In addition, all the parts mentioned above, together with the objective lens, constitute our optical device which has a lateral resolution of 14 μm and an object field of view of $1.2 \times 1.0\,\mathrm{cm}^2$.

When the device works, the light emitted from the LED is reflected by the 45° dichroic filter and shines on the skin. Then the fluorescence excited from the skin transmits through the 45° dichroic filter and is captured by the image sensor. Therefore, the reflected excitation source and the fluorescence have the same optical path. Such a design can not only minimize the whole device and lower the energy consumption, but also eliminate the homogeneity problem of illumination and fluorescence imaging. The prototype of our fluorescence imaging device is shown in Fig. 2(a). The total volume of our device is smaller than $116\,\mathrm{cm}^3$ ($3.5 \times 3.5 \times 9.5\,\mathrm{cm}^3$), with a weight of 150 g and a consumption power of 1.5 W. Its size is reduced to be smaller than a cell phone. The overview of our experiment system is shown in Fig. 2(b). The total volume is very small and similar to the camera part reported by Kulyk *et al.* (2015).[22] They adopted a ring light source as the excitation source around the camera (LM075 M). Their cameras volume is $108\,\mathrm{cm}^3$ ($4.4 \times 4.4 \times 5.6\,\mathrm{cm}^3$), with a weight of 130 g and a consumption power of 2.5 W if regardless of the ring light source part. However, if their ring light source is taken into account, its volume looks three times larger than ours. The weight and power consumption of our devices are also significantly smaller than theirs. Furthermore, their lighting power generated from 16 LEDs is only $0.1\,\mathrm{mW/cm}^3$, which is proportional to the excited fluorescence signal. As a comparison, the lighting power of our device can reach $19.8\,\mathrm{mW/cm}^3$ with only one LED, which can have a much stronger excited fluorescence signal and much easier to detect the tumor. These data are listed in Table 1.

(a)

(b)

Fig. 2. Experimental system. (a) is the device compared with a cell phone. (b) is the overview of our experimental system.

Table 1. Parameters of fluorescence imaging device.

Type	Volume	Weight	Consumption power	Number of the LED	Lighting power
Ours	116 cm^3 (total)	150 g (total)	1.5 W (total)	1	19.8 mW/cm^3
Reported by O. Kulyk *et al.*	108 cm^3 (Regardless of the ring light source)	130 g (Regardless of the ring light source)	2.5 W (Regardless of the ring light source)	16	0.1 mW/cm^2

3. Materials and Methods

In order to verify the feasibility of the miniaturized fluorescence imaging system, the experiment was designed to take fluorescence images of mice skin tumors. The experiment site located in the Shanghai Dermatology Hospital, experimental subjects and procedure will be described in detail as follows.

3.1. *Animal model*

Female, hairless SKH-1 mice (6–8 weeks old) were obtained from the Jackson Laboratory. In our study, the mice were divided into two groups: One was the cutaneous squamous cell carcinoma (cSCC) mice group, and the other was a normal control group. In each group, some mice were taken out and applied with 10% ALA cream, and the other mice were not applied. The methods of obtaining cSCC mice and applying ALA cream are introduced as follows.

The squamous cell carcinoma mice were obtained as follows. We took one cage mice (there were 5 mice each cage), and adjusted the exposure light source (SS-03B UV-B Phototherapy armarium with exposure power of 0.26 mW/cm^2) to about 30 cm from the back of the mouse. The exposure light was illuminated on the back of the mice by 2 min a time, five times a week (from Monday to Friday). This process lasted 20–24 weeks, until tumors with a diameter of about 5 mm appeared, and the cumulative UVB dose was approximately 1.59 J/cm^2. The experiment mice are shown in Fig. 3. The tumor had been fully discussed in our previous work[27,28] which also included the histopathological examination and the electron microscopic examination. There are a lot of appearances shown in the histopathological results of mouse squamous cell carcinoma: Hyperkeratinization, irregular epidermal hyperplasia, a large number of atypical cells, obvious mitosis figures, the appearance of keratinized cells and horns, some tumor tissues break through the basement membrane to the dermal reticular layer. All of these prove that the mouse cSCC is consistent with the pathology of human cSCC, and can be used as a verification of the presurgical experiment of skin squamous cell carcinoma.

The method of applying ALA was as follows. First, we anesthetized the mice, then applied 10% ALA cream to them with cotton balls, and last, immediately placed the mice in a dark room to avoid light for 2 h.[27,28] For the cSCC mice, the ALA solution was topically applied on and around the tumor, and for normal mice, the application area corresponded to that of the cSCC mice.

3.2. *Parameter adjustment of the fluorescence imaging system*

In order to adjust the parameters of the fluorescence imaging system, we needed to take images of the malignant tumor which was visible to the eyes. In this experiment, a cSCC mouse applied with ALA cream was chosen. The mouse was anesthetized

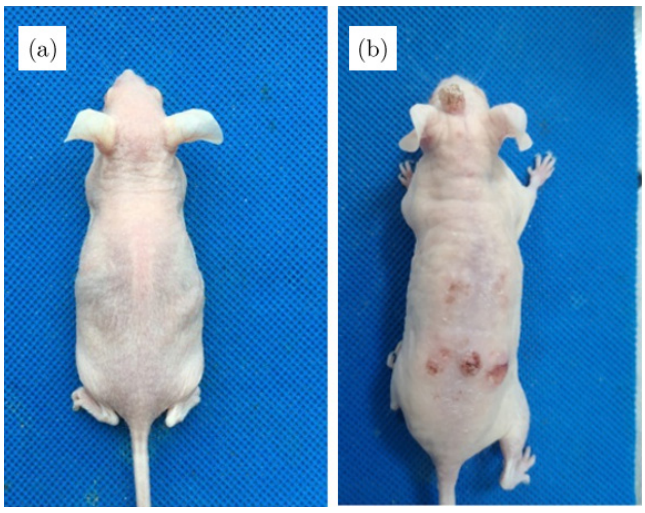

Fig. 3. (a) control group, (b) squamous cell carcinoma mice group.

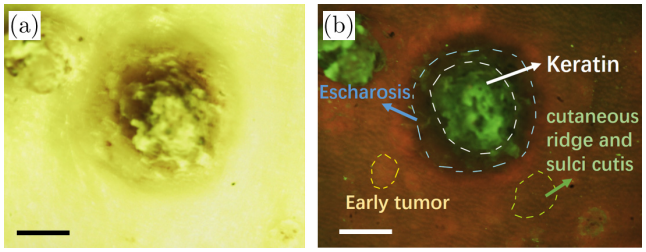

Fig. 4. (a) White light image of malignant squamous cell carcinoma tumor, scale bar: 2 mm. (b) Fluorescent image of malignant squamous cell carcinoma tumor, scale bar: 2 mm.

with an anesthesia machine and the lesion was placed directly under the fluorescence imaging system. The exciting LED was turned off and the white lamp on the roof was turned on when taking the white light images. Only the 405 nm LED exciting light in the imaging device was turned on when taking a fluorescent image. The imaging results are shown in Figs. 4(a) and 4(b).

The results show that both the white light and fluorescent tumor images can be captured by the device clearly. The white light images display a strong yellow-green background because the high-pass filter can block blue light out. Moreover, the fluorescent images can show the information of normal skin, early tumor areas and malignant tumor lesions more clearly, compared with the white light images. In the fluorescent image, the texture of skin can be clearly displayed as shown in Fig. 4(b). The convex part is the cutaneous ridge and the concave part is the sulci cutis. The ridge presents a thin strip of red in the fluorescent image while the sulci cutis shows dark gray. The early tumors were reddish. It is difficult to distinguish the sulci and ridge of tumors. There were keratin and escharosis in the malignant tumor. The keratin was bright green and the escharosis was black. Part of the point green fluorescence was from dander.

This result demonstrates that the miniaturized fluorescence imaging device is capable of collecting skin information well under both white light and fluorescent conditions. Also, the experiment parameter is confirmed as follows: The height of the camera in the experiment is 9.5 cm. The imaging area is 1.2 cm × 1.0 cm. The electrical consumption power of LED is 1 W. And the integration time of the camera is 0.11 s, which is very fast for catching images and diagnosis. Owing to the miniature size of the device with coaxial path design for illumination and fluorescence, one can take both the white light and fluorescence pictures of almost any position easily and rapidly.

Table 2. Parameters of fluorescence imaging device.

Groups	Experimental group		Control group	
Types	ALA	None_ALA	ALA	None_ALA

3.3. *Early tumors detection*

After completing the parameter adjustment of the fluorescence imaging system, an experiment was arranged to explore the effect of the fluorescence imaging device in early tumor detection. In the experiment, we took two squamous cell carcinoma SKH-1 mice as an experimental group and chose invisible lesions as the test area. Then, we took two normal SKH-1 mice as a control group and chose the same part in the experimental group as contrast area. There were two mice in the experimental group. One was applied with ALA for 2 h while the other was not applied. The control group is the same as the experimental group. The classification of the mice is shown in Table 2.

4. Results and Discussion

We take fluorescence images and white light images of early skin tumors in the primary tumor group. The images of the skin taken by our device are shown in Fig. 5. Figure 5(a) is the skin under white light and not treated with ALA. Figure 5(b) is the skin under white light but treated with ALA. It can be seen that under the white light, the color and texture of early tumors and normal skin are similar, no matter they are treated with ALA or not. Therefore, it is hard to distinguish the early tumor site from normal skin with the naked eye for normal illumination.

Figure 5(c) shows the green fluorescence image of mouse skin under the LED light without being treated with ALA, but no early tumors can be distinguished from normal skin. The small bright green dots in the figure may be the fluorescence of collagen or scurf excited by LED. After finishing the ALA treatment and then capturing the fluorescence image under the LED light, the early tumor shows a bright red fluorescence spot which is in obvious contrast to normal skin, as shown in Fig. 5(d). Red

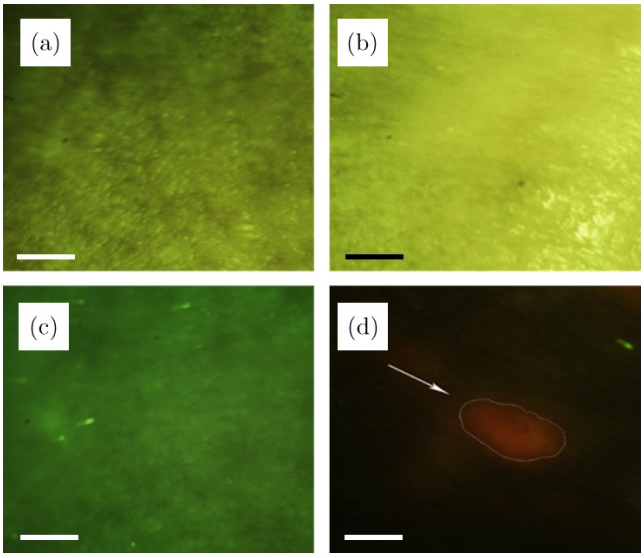

Fig. 5. Fluorescence images and natural light images of early skin tumors in the primary tumor group. (a) ALA-free natural light image, (b) ALA-treated natural light image, (c) ALA-free fluorescence image, (d) ALA-treated fluorescence image. All of the scale bars are 1 mm.

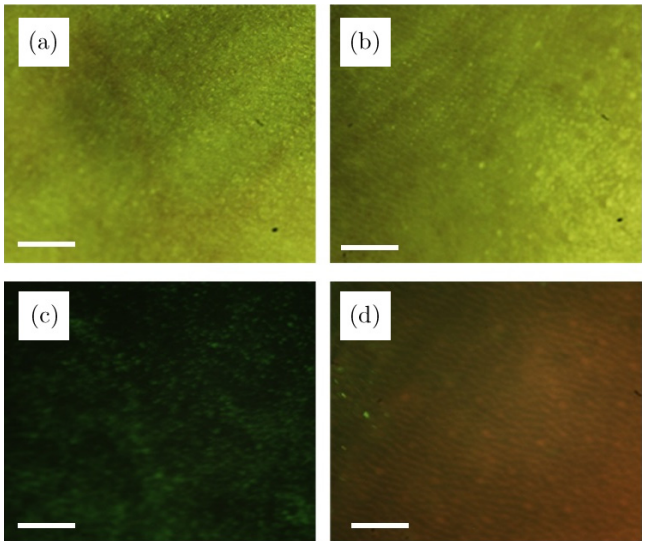

Fig. 6. Fluorescence images and natural light images of normal skin in the control group. (a) ALA-free natural light image, (b) ALA-treated natural light image, (c) ALA-free fluorescence image, (d) ALA-treated fluorescence image. All of the scale bars are 1 mm.

spots are the images of early tumors diagnosed by the doctors of Xinhua Hospital. Therefore, the early tumor can be easily distinguished from normal skin by fluorescence imaging after treated with ALA. It can be easily used for early tumor diagnosis rapidly with noninvasion since the time of imaging an area of 1.2 cm × 1.0 cm needs only 0.11 s.

To verify the practicability and validity of our fluorescence image device, the control experiment was designed. We chose the normal mice mentioned in Sec. 3.2.2 as the control group and took fluorescence images under the same experimental conditions as before. The results are shown in Fig. 6. Figure 6(a) is the skin under white light and not treated with ALA. Figure 6(b) is the skin under white light but treated with ALA. Figure 6(c) shows the green fluorescence image of mouse skin under the LED light without treated with ALA, and there is no significant difference compared with Figs. 5(a)–5(c). They reveal that the tumor cannot be distinguished under white light or under LED without ALA treated. Figure 6(d) shows the fluorescence image of mouse skin under the LED light and treated with ALA, the red cutaneous ridge and dark sulci cutis can be seen from it. But there is no bright red spot like Fig. 5(d). Therefore, red spots exist only in experimental mice, further indicating that the red spots are tumor images and demonstrating the validity of our fluorescence imaging device.

As a result, there is no significant difference between the experimental group and the control group in the case of white light or LED light but not ALA-treated. However, under the LED light and being treated with ALA, there are obvious red spots only in the experiment mouses fluorescence images. One can distinguish and locate the cancer tumor from it according to these spots.[29] Moreover, the sulci and ridge of normal skin can be clearly exhibited by the fluorescent image after treated with ALA. In a word, our device can detect the early skin tumors and locate them in real-time on a large scale.

5. Conclusion

In this paper, we propose a novel miniature fluorescence imaging device with a coaxial optical path design. The coaxial light source is artfully embedded in the device with a 45° dichroic, which significantly reduces the size of the device while ensuring the illumination homogeneity. The total volume of the device is less than $3.5 \times 3.5 \times 9.5\,\text{cm}^3$, which is only similar to the reported camera part regardless

of the ring light source. The weight of our device is 150 g with a consumption power of only 1.5 W, while the lighting power can reach 19.8 mW/cm^2. Besides, 480 nm short-pass and 503 nm long-pass filters have also been utilized in the device to further reduce the stray light and enhance the signal-to-noise ratio (SNR). To verify the validity of our device, it is used to detect the skin cancer tumor. The results show that our device can be used to clearly and rapidly distinguish the lesion and locate the tumor. To our best knowledge, the fluorescence imaging device we reported is the most compact one to detect the early skin cancer tumor with much lower consumption power. It is very convenient to be held, and can detect skin surface on a large scale rapidly. Moreover, the device is prospective to be integrated with an ultrasound probe to achieve multi-mode detection of tumors, which can increase the diagnosis accuracy remarkably.

Conflict of Interest

The authors declare no conflict of interest.

Acknowledgments

Jingyue Pan and Qingquan Liu authors contributed equally to this work. This work was funded by the Development Program of China (973 Program) [2017YFC0111400], National Natural Science Foundation of China (NSFC) [11874376], Shanghai Science and Technology Foundation [18590712600, 18DZ2282200, 19DZ2293400, 19ZR1465900], Shanghai Municipal Science and Technology Major Project (2019SHZDZX01).

References

1. U. Leiter, U. Keim, T. Eigentler, A. Katalinic, B. Holleczek, P. Martus, C. Garbe, "Incidence, mortality, and trends of nonmelanoma skin cancer in Germany," *J. Invest. Dermatol.* **137**(9), 1860–1867 (2017).
2. D. S. Rigel, "Commentary: The incidence of nonmelanoma skin cancer," *J. Amer. Acad. Dermatol.* **71**, 27–28 (2014).
3. H. W. Rogers, M. A. Weinstock, S. R. Feldman, B. M. Coldiron, "Incidence estimate of nonmelanoma skin cancer (keratinocyte carcinomas) in the US population, 2012," *JAMA Dermatol.* **151**, 1081–1086 (2015).
4. F. Xiang, R. Lucas, S. Hales, R. Neale, "Incidence of nonmelanoma skin cancer in relation to ambient uv radiation in white populations, 1978–2012 empirical relationships," *JAMA Dermatol.* **150**, 1063–1071 (2014).
5. A. Stang, L. Khil, H. Kajer, N. Pandeya, C. Schmults, E. Ruiz, P. Karia, A. Green, "Incidence and mortality for cutaneous squamous cell carcinoma: Comparison across three continents," *J. Eur. Acad. Dermatol. Venereol.* **33**(S8), 6–10 (2019).
6. C. T. Andrade, J. D. Vollet-Filho, A. G. Salvio, V. S. Bagnato, C. Kurachi, "Identification of skin lesions through aminolaevulinic acid-mediated photodynamic detection," *Photodiagn. Photodyn. Therapy* **11**, 409–415 (2014).
7. W. P. Coleman, III, "Skin cancer: Recognition and management, 2nd Edition," *Dermatol. Surg.* **34**, 1702 (2008).
8. A. Esteva, B. Kuprel, R. A. Novoa, J. Ko, S. M. Swetter, H. M. Blau, S. Thrun, "Dermatologist-level classification of skin cancer with deep neural networks," *Nature* **546**, 686 (2017).
9. E. Errichetti, G. Stinco, "Dermoscopy in general dermatology: A practical overview," *Dermatol. Therapy* **6**, 471–507 (2016).
10. M. A. Calin, S. V. Parasca, R. Savastru, M. R. Calin, S. Dontu, "Optical techniques for the noninvasive diagnosis of skin cancer," *J. Cancer Res. Clin. Oncology* **139**, 1083–1104 (2013).
11. K. S. Nehal, D. Gareau, M. Rajadhyaksha, "Skin imaging with reflectance confocal microscopy," *Semin. Cutan. Med. Surg.* **27**, 37–43 (2008).
12. A. Bezugly, "High frequency ultrasound study of skin tumors in dermatological and aesthetic practice," *Med. Ultrason.* **17**, 541–544 (2015).
13. M. L. Marino, T. Rogers, H. S. Gil, M. Rajadhyaksha, M. A. Cordova, A. A. Marghoob, "Improving lesion localization when imaging with handheld reflectance confocal microscope," *Skin Res. Technol.* **22**, 519–520 (2016).
14. A. Lallas, I. Zalaudek, E. Moscarella, C. Longo, H. P. Soyer, G. Argenziano, "The dermatologist's stethoscope — traditional and new application of dermoscopy," *Dermatol. Pract. Concept.* **3**(2), 67–71 (2013).
15. C. Hu, H. Cai, Z. Xing, T. Li, Application of photodynamic fluorescence diagnosis in skin tumors, *Applied Laser* **38**(4), 701–704 (2018).
16. Y. Matoba, K. Banno, I. Kisu, D. Aoki, "Clinical application of photodynamic diagnosis and photodynamic therapy for gynecologic malignant diseases:

A review," *Photodiagn. Photodyn. Therapy* **24**, 52–57 (2018).

17. Y.-T. Lin, Y.-C. Hsiao, Y.-F. Chiang, C.-J. Chang, "Topical application of photofrin® for photodynamic diagnosis of malignant cutaneous neoplasms," *J. Plast. Reconstr. Aesthet. Surg.* **71**, 1487–1495 (2018).
18. Y. Nakai, K. Inoue, T. Tsuzuki, T. Shimamoto, T. Shuin, K. Nagao, H. Matsuyama, M. Oyama, H. Furuse, S. Ozono, M. Miyake, K. Fujimoto, "Oral 5-aminolevulinic acid-mediated photodynamic diagnosis using fluorescence cystoscopy for non-muscle-invasive bladder cancer: A multicenter phase III study," *Int. J. Urol.* **25**, 723–729 (2018).
19. L. E. Simonato, S. Tomo, R. Scarparo Navarro, A. G. J. Balbin Villaverde, "Fluorescence visualization improves the detection of oral, potentially malignant, disorders in population screening," *Photodiagn. Photodyn. Therapy* **27**, 74–78 (2019).
20. J. Wizenty, T. Schumann, D. Theil, M. Stockmann, T. Wuensch, "Recent advances and the potential for clinical use of autofluorescence detection of extra-ophthalmic tissues," *Molecules* **25**(9), 2095 (2020).
21. S. Tomo, G. I. Miyahara, L. E. Simonato, "History and future perspectives for the use of fluorescence visualization to detect oral squamous cell carcinoma and oral potentially malignant disorders," *Photodiagn. Photodyn. Therapy* **28**, 308–317 (2019).
22. O. Kulyk, S. H. Ibbotson, H. Moseley, R. M. Valentine, I. D. W. Samuel, "Development of a handheld fluorescence imaging device to investigate the characteristics of protoporphyrin IX fluorescence in healthy and diseased skin," *Photodiagn. Photodyn. Therapy* **12**, 630–639 (2015).
23. C. Grecco, H. H. Buzza, M. D. Stringasci, C. T. Andrade, J. D. Vollet-Filho, S. Pratavieira, A. L. Zanchin, A. M. Tuboy, V. S. Bagnato, Single led-based device to perform widefield fluorescence imaging and photodynamic therapy, in *Biophotonics South America, International Society for Optics and Photonics*, p. 953121, (2015).
24. Z.-C. Zhao, Y. Zhou, G. Tan, L. Juan, "Research progress about the effect and prevention of blue light on eyes," *Int. J. Ophthalmol.* **11**(12), 1999–2003 (2018).
25. K. Hayashi, H. Uhara, R. Okuyama, "Detection of the tumor margin of basal-cell carcinoma using dermoscopy and high-frequency ultrasound with narrow pieces of surgical tape as skin markers," *Dermatologic Surgery* **40**(6), 704–706 (2014).
26. L. Lovatto, C. Carrera, G. Salerni, L. Alos, J. Malvehy, S. Puig, "In vivo reflectance confocal microscopy of equivocal melanocytic lesions detected by digital dermoscopy follow-up," *J. Eur. Acad. Dermatol. Venereol.* **29**, 1918–1925 (2015).
27. X. Wang, L. Shi, Q. Tu, H. Wang, H. Zhang, P. Wang, L. Zhang, Z. Huang, F. Zhao, H. Luan, X. Wang, "Treating cutaneous squamous cell carcinoma using 5-aminolevulinic acid polylactic-co-glycolic acid nanoparticle-mediated photodynamic therapy in a mouse model," *Int. J. Nanomed.* **10**, 347–355 (2015).
28. J. Ji, P. Wang, Q. Zhou, L. Zhu, H. Zhang, Y. Zhang, Z. Zheng, A. K. Bhatta, G. Zhang, X. Wang, "CCL8 enhances sensitivity of cutaneous squamous cell carcinoma to photodynamic therapy by recruiting M1 macrophages," *Photodiagn. Photodyn. Therapy* **26**, 235–243 (2019).
29. J. de Leeuw, N. van der Beek, W. D. Neugebauer, P. Bjerring, H. A. M. Neumann, "Fluorescence detection and diagnosis of non-melanoma skin cancer at an early stage," *Lasers Surg. Med.* **41**, 96–103 (2009).